Spectroscopic signature of sublattice polarization in the lattice dynamics of an antiferroelectric crystal

E. Constable [1,*] L. Bergen [1] A. Shuvaev [1] J. Wettstein [1] L. Weymann [1] E. Malysheva,[1]
A. Pimenov [1] and M. Guennou [2,†]

[1]*Institute of Solid State Physics, TU Wien, 1040 Vienna, Austria*
[2]*Department of Physics and Materials Science, University of Luxembourg, 41 rue du Brill, L-4422 Belvaux, Luxembourg*

Spectroscopic measurements of the far-infrared phonon dynamics for a model antiferroelectric crystal are performed at low temperature. In agreement with the phenomenological expectations for a displacive antiferroelectric transition, a polar soft mode associated to a close-lying polar phase of the otherwise centrosymmetric structure is observed. Incomplete softening of the polar soft mode due to the antiferroelectric transition quantifies the energy barrier between the neighboring states. The dynamics are modeled with a biquadratic Landau potential incorporating a symmetry constraining effective interaction between displaced ions. A signature of sublattice polarization is observed in a scaling of the effective antipolar interaction in the antiferroelectric phase.

The intuitive notion of antiferroelectricity, as laid out in Kittel's seminal paper [1] and many subsequent works (e.g., Refs. [2,3]), is rooted in the concept of *sublattice polarization*, i.e., the idea that one can identify a *dipolar structure* in an antiferroelectric (AFE) crystal such that (i) the total (average) polarization cancels out in the absence of an electric field, the so-called *antipolar* phase, and (ii) each sublattice can be controlled or "switched" by an electric field, inducing a polar phase transition with characteristic double-hysteresis *P–E* loops. In the most general sense, such an image is not strictly valid, as any ionic crystal can be decomposed into subregions with apparent opposite polarization [4,5]. Yet, it is certainly practical when elements carrying an electric dipole are naturally identified in a structure, such as in AFE molecular [6] or liquid crystals [7]. Moreover, it makes sense to consider the emergence of polarized sublattices in the context of phase transitions involving a symmetry descent from a parent to a lower-symmetry phase with local breaking of inversion symmetry [8].

In principle, for a proper AFE transition, sublattice polarization is the primary order parameter that emerges below the critical temperature T_c. It therefore represents the key quantity to monitor in AFE systems, although it is rarely done. For one thing, sublattice polarization cannot be measured by integrating transient currents (as is done for ferroelectric polarization), and thus it is never in fact quantified directly. Instead, other quantities like ion displacements are used as a proxy, or the evolution of the saturation polarization seen

in the *P–E* double loop is monitored as a function of temperature. Often, the requirement for large poling fields, and the common occurrence of spurious currents with origins other than polarization reversal means this approach is not always possible. Moreover, in the case of displacive AFE transitions specifically, there are a lack of suitable model systems for which the order parameter is well defined. Indeed, many of the commonly studied AFE crystals are either of the order-disorder type [9,10], or are very complex with multiple interacting order parameters, sublattice polarization being essentially improper in these cases. The latter applies in particular to the model AFE perovskite $PbZrO_3$ [11–13], whose electric-field-induced transition is far more complex that the simple flipping of a polarization sublattice as envisioned in a Kittel AFE. Thus, there is a strong motivation to find new models, and specifically an AFE equivalent of the famous displacive ferroelectric (FE) $PbTiO_3$.

Recent work has shown that francisite $[Cu_3Bi(SeO_3)_2O_2Cl]$ might just fill this gap. Aside from a novel antiferromagnetic order below $T_N = 25$ K, francisite features a structural phase transition at ~ 118 K [14]. Its low-energy phonon dispersion reveals this to be driven by an antipolar vibrational soft mode at the Brillouin-zone boundary [15]. This discovery highlights a rare example, where a single zone-boundary (antipolar) phonon drives a purely displacive phase transition in one dimension. The simplistic one-dimensional symmetry descent (see Fig. 1), accompanied by a dielectric anomaly, fits within an antipolarized sublattice description [14]. At the same time, structural computations show that a close-lying polar phase is nearly degenerate to the antipolar ground state [15,16]. Together, these indicators provide strong evidence that francisite is indeed a model example of a displacive AFE. In this scenario, we expect that the antipolar soft mode representing out-of-phase oscillations of the ions associated to the polarized sublattice is connected via the phonon dispersion to a zone-center polar mode representing in-phase oscillations of the same ions [17,18]. Thus,

---
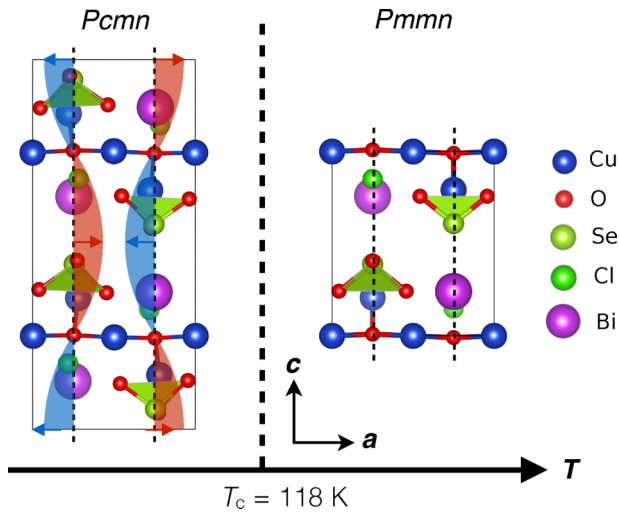*evan.constable@tuwien.ac.at
†mael.guennou@uni.lu

FIG. 1. *ac*-plane crystal structure of francisite showing antipolar distortion of parent *Pmmn* (No. 59) phase to lower-symmetry *Pcmn* (No. 62) phase below $T_c \approx 118$ K. Red and blue shaded areas exaggerate the atomic displacements below T_c.

a polar soft mode should also be visible in the low-frequency infrared spectrum of francisite, evidence that is so far lacking.

In this Letter, we perform an infrared (IR) study of francisite, extending the previously investigated frequency range [19] into the sub-THz domain. The results show clear evidence of a polar soft mode consistent with a zone-center extrapolation of its antipolar counterpart. Moreover, we show that both modes are well described by a one-dimensional second-order displacive model, from which a signature of the sublattice polarization can be obtained. Together these results further support the argument towards francisite as a textbook example of an ideal displacive AFE.

Far-IR reflectivity and complex THz transmission measurements of francisite were performed on a thin single-crystal sample, with dimensions $\sim 5 \times 5 \times 0.1$ mm^3, grown using the chemical vapor-phase method described in Ref. [19]. The primary face of the sample was normal to the $\hat{c}$ axis and the optical polarization was fixed $\mathbf{e} \parallel \hat{a}$ to probe the lattice dynamics along the antiferrodistortive axis. The reflectivity measurements were performed using a Bruker Vertex 80v Fourier-transform infrared (FTIR) spectrometer. The transmission measurements we performed using backwards wave-oscillator sources implemented in a Mach-Zehnder (MZ) interferometer. Spectra were obtained at 13 temperatures between 10 and 300 K. Further experimental details can be found in the Supplemental Material along with broadband spectra covering the frequency range 8–900 cm^{-1} [20].

The *a*-axis reflectivity between 8 and 120 cm^{-1} is shown in Fig. 2(a). Spectra at three characteristic temperatures are featured: One below both the magnetic (T_N) and structural (T_c) phase transitions (10 K), one in proximity to T_c (120 K), and one above T_c (300 K). Data points from 40–120 cm^{-1} are the experimental results of the FTIR measurements. Data points from 8–28 cm^{-1} are from the MZ interferometer. The complex transmission measurements of the MZ interferometer have been converted to reflectivity to help analyze the FTIR data into the sub-THz range. This was achieved by
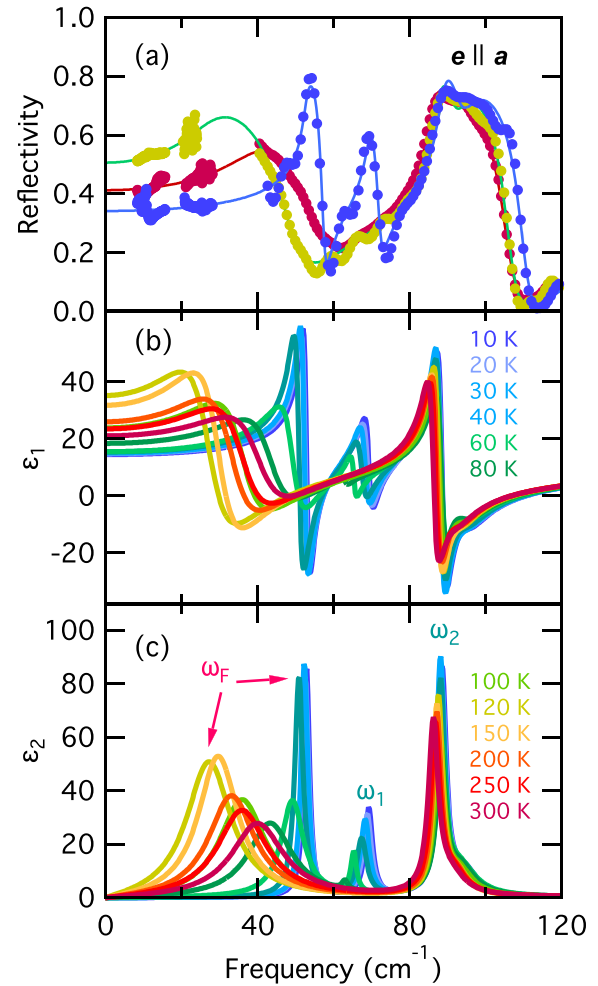

FIG. 2. Low-energy IR lattice dynamics in francisite. The experimental reflectivity (a) is used to extract the real (b) and imaginary (c) components of the dielectric permittivity. Labels indicate the different phonon contributions to the Lorentzian oscillator model of Eq. (2).

converting the measurements of transmission and phase into a complex permittivity ($\varepsilon = \varepsilon_1 + i\varepsilon_2$) and then applying the following Fresnel equation describing single bounce reflectivity at normal incidence,

$$R(\omega) = \left| \frac{1 - \sqrt{\varepsilon(\omega)}}{1 + \sqrt{\varepsilon(\omega)}} \right|^2. \qquad (1)$$

Solid lines in Fig. 2(a) are theoretical fits using Eq. (1) and an underdamped Lorentz-oscillator model of the form

$$\varepsilon(\omega) = \varepsilon_\infty + \sum_i \frac{\Delta \varepsilon_i \omega_i^2}{\omega_i^2 - \omega^2 - i\gamma_i \omega}. \qquad (2)$$

Here, $\Delta \epsilon_i$ represents the oscillator strength, ω_i the frequency, and γ_i the damping (full width at half-maximum) of the *i*th Lorentzian-oscillator phonon mode. The fitting was performed using a Marquardt-Levenberg least-squares procedure within the WAVE METRICS IGOR PRO software package. The high-frequency contribution to the permittivity ($\epsilon_\infty = 4.2$) was held constant to improve fitting stability and is justified

by the static reflectivity above ∼850 cm^{-1} observed over all temperatures.

We note that the uncertainties of the fits determined by a covariance matrix implemented in the least-squares fitting algorithm will typically underestimate the true experimental error of the measurements [25]. Thus, the uncertainty in frequency position was further approximated by taking the half-width at half-maximum value of the corresponding peak. The uncertainty for the dielectric contribution for each oscillator was approximated by considering a 5% uncertainty in its reflectivity contribution, a modest assumption based on observations of repeatability of the reflectivity measurements.

Despite the onset of antiferromagnetic order below 25 K [14], the magnetic permeability was held constant at $\mu = 1$ in all fits. A small peak in the 10-K reflectivity at ∼11 cm^{-1} is attributed to antiferromagnetic resonance in the permeability channel of the complex transmission measurements. We note that this magnetic contribution should not appear with this profile and strength in reflectivity but found that it had negligible consequence on the fitting of $\varepsilon(\omega)$ compared to the far more dominant lattice dynamics.

The real and imaginary components of the dielectric permittivity extracted from the reflectivity fits are shown in Figs. 2(b) and 2(c). The spectrum is dominated by a strongly damped oscillator at ∼40 cm^{-1} that softens with decreasing temperature. Below T_c, it starts to harden and becomes less damped. This behavior is reminiscent of the low-frequency phonon dynamics of other notable AFE candidates such as Rochelle salt [26] and PbZrO$_3$ [27].

The damped profile and frequency softening is indicative of a polar lattice instability. While attempts were made to fit this mode with an overdamped oscillator of the Debye form, it was found that the Lorentz model gave the best fit for all temperatures investigated. The absence of complete softening and significantly overdamped or "central mode" behavior [28] is a strong indication that the structural transition at T_c is essentially displacive as proposed by Milesi-Brault *et al.* [15].

The temperature dependence of the fitted oscillator parameters and their uncertainties are given in Fig. 3. Here, the lowest-energy mode designated ω_F clearly features the most prominent changes in relation to the other phonons. Specifically, the frequency (ω_F) softens to about 50% of its 300-K value at T_c. It then hardens significantly at lower temperatures while none of the other phonons shift in frequency by more than 5% across the entire temperature span. The damping (γ_F) is also unique, demonstrating a rapid shift from critical damping as $\omega_F \rightarrow \gamma_F$ above T_c to underdamping below ∼80 K. Finally, the oscillator strength ($\Delta\varepsilon_F$) representing the primary contributor to the static permittivity exhibits a characteristic anomaly at T_c. The sum of all the dielectric contributions (including ε_∞) is in excellent agreement with the low-frequency capacitive measurements obtained at 100 kHz using an alpha-analyzer and Physical Properties Measurement System (PPMS) [20]. This gives strong support to our fitting model and highlights the primary role ω_F plays in the dielectric response of the $\hat{a}$-axis antipolar transition.

So far, the characteristic double-hysteresis P–E loop used to identify a close-lying FE phase has not been observed for francisite. Attempts were made by measuring the charge buildup on silver painted electrodes as a function of volt-
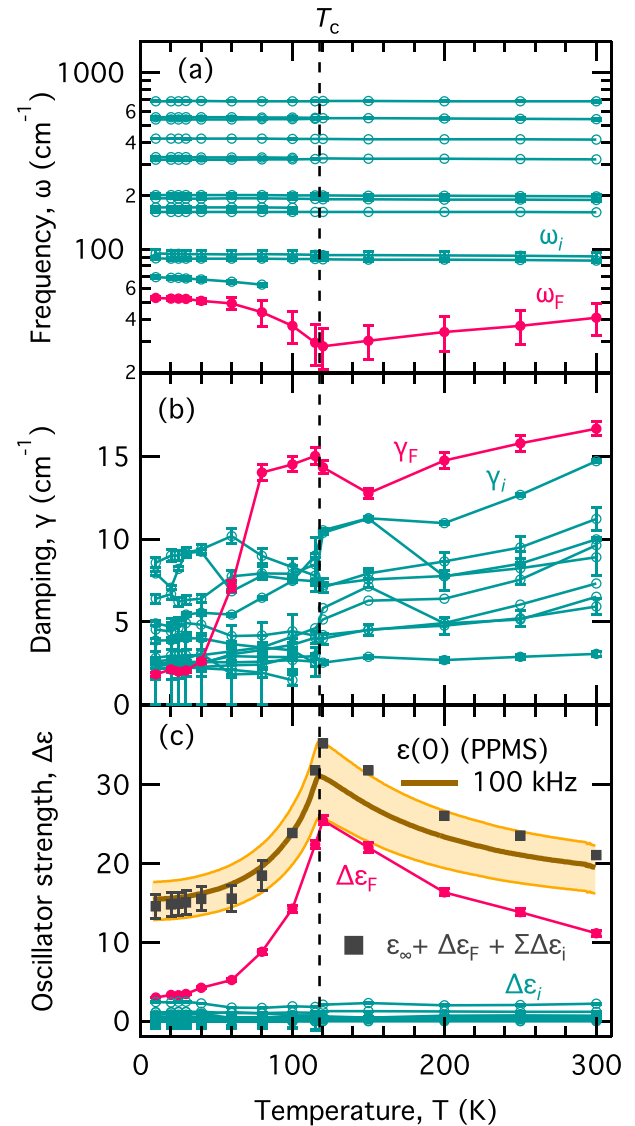

FIG. 3. Temperature dependence of fitted oscillator parameters. The soft mode is highlighted (rose) relative to the other more static lattice modes (teal). The yellow shaded area in (c) represents a geometric calibration uncertainty for the capacitance measurements (see [20–24] for details).

age applied along the $\hat{a}$ direction [20]. Voltage sweeps up to ±80 kV/m were performed at several temperatures above and below T_c. Electrical discharge across the sample inhibited higher field strengths. No clear signature of an electrically induced FE or ferrielectric phase was observed, but we note that the maximum field achieved here lies well below typical antiferroelectric switching fields [29].

In the absence of an electric-field induced transition, we look to the IR lattice dynamics for insight regarding a potential neighboring polar phase. A displacive AFE transition should be accompanied by a FE soft mode that represents the Γ point of the antipolar soft-mode band [18]. The energy difference between the Γ point and boundary point of the phonon dispersion determines if a FE or AFE phase is ultimately stabilized.

This is in precise agreement with our IR observations for **e** ∥ $\hat{a}$ and the polar soft-mode behavior of ω_F. At 300 K,
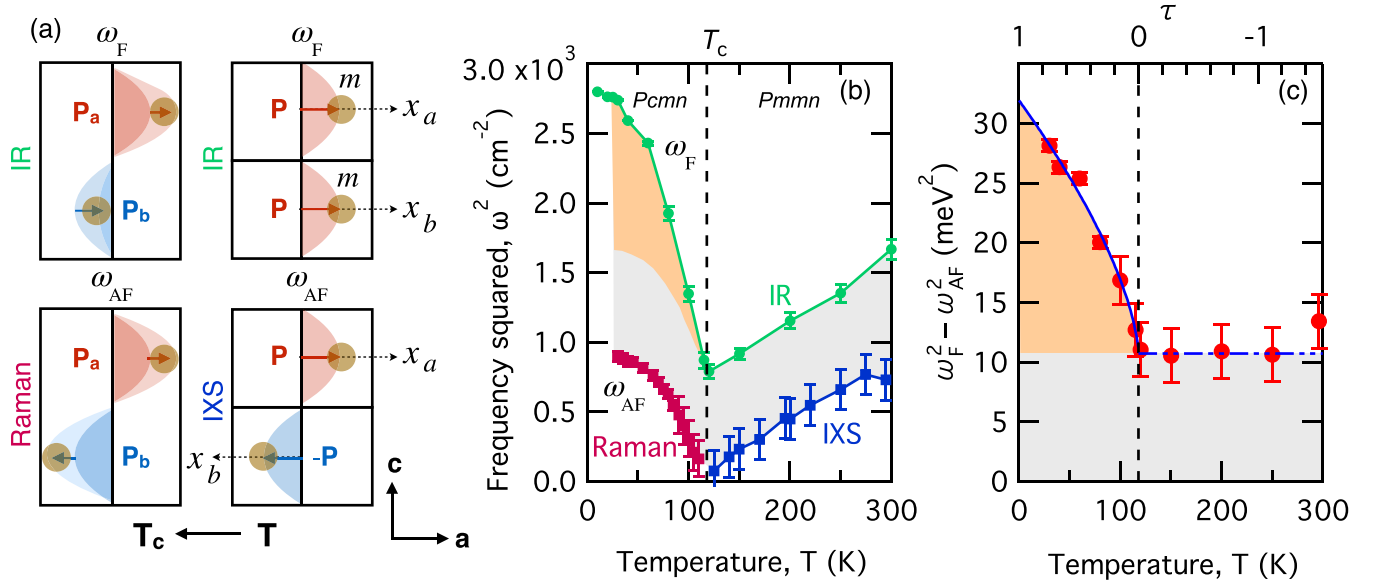
FIG. 4. (a) Simplified diagram of local polar moments carried by the FE (ω_F) and AFE (ω_{AF}) soft modes. Each displacement x_a and x_b behaves independently in its local potential [Eq. (3)], only interacting through the model potential [Eq. (5)]. (b) Squared frequency dependence of ω_F obtained using IR techniques described in the text and ω_{AF} adapted from Ref. [15] obtained using inelastic x-ray scattering (IXS) and Raman spectroscopy. (c) The difference of ω_F^2 and ω_{AF}^2 is proportional to the model interaction potential revealing a signature of the AFE sublattice polarization below T_c (orange shaded area).

$\omega_F = 41 \, \text{cm}^{-1}$ while the antipolar soft mode $\omega_{AF} = 27 \, \text{cm}^{-1}$, as determined by inelastic x-ray scattering in Ref. [15]. The dispersion band of ω_{AF} mapped from the Z point towards the Γ point in Ref. [15] increases in energy and intercepts our observation of ω_F close to the Γ point. Thus, we identify ω_F as the polar mode for the neighboring FE phase. We can then use the incomplete softening of ω_F at T_c as a probe of the energy barrier between the FE and AFE phases. Taking the displaced Cl$^-$ ions as the primary ionic distortion below T_c (see Ref. [20]), we estimate that electric fields of the order of ~ 1.2 MV/m are required to switch francisite to its polar phase in the vicinity of T_c.

A key observation of Ref. [15] [see Fig. 4(b)] is how the temperature evolution of the antipolar soft mode in francisite follows Cochran's model of displacive transitions, i.e., $\omega_{AF}^2 \propto (T - T_c)$ [17,30]. This indicates that the antipolar distortion, confined largely to a single crystallographic axis, occurs due to a local lattice instability.

We can model a simple one-dimensional instability with a biquadratic Landau potential

$$U(x) = ax^2 + bx^4, \qquad (3)$$

where x is the ionic displacement and $a(T) = \alpha(T - T_c)$. Antipolar instability is achieved by considering two equivalent masses ($m_a = m_b = m$), each within a local potential [Eq. (3)], and constrained along two independent parallel axes x_a and x_b as in Fig. 4(a). Here, we can select for polar or antipolar symmetry by including an "effective interaction" potential

$$U_F = c(x_a - x_b)^2, \qquad (4)$$

$$U_{AF} = c(x_a + x_b)^2. \qquad (5)$$

The total potential experienced by each mass is $U_{tot} = U(x_{a,b}) + U_{F,AF}$. Ferroelectric ($U_F$) or AFE ($U_{AF}$) order is selected depending on the choice of interaction and by fixing $x_a = x_b$ for the FE and $x_a = -x_b$ for the AFE case. The eigenmodes describing the dynamics of this model are derived in the Supplemental Material [20] and summarized in Table I.

Naturally, the behavior of the polar eigenmode for FE ordering is nothing but the well-documented *ferroelectric soft mode* with an order parameter of spontaneous polarization given by $P = qnx$, where q and n are the charge and density of the displaced ion. Interestingly, the antipolar mode is gapped relative to the polar mode by an amount proportional to the interaction potential. The situation is reversed for AFE ordering. Thus, considering all other parameters equal (mass, charge, density), the difference between the squared frequencies of the polar and antipolar modes for each type of ordering is directly proportional to the strength of the interaction potential $\omega_F^2 - \omega_{AF}^2 \propto c$.

The temperature evolution of ω_F^2 and ω_{AF}^2 in francisite is shown in Fig. 4(b). In a previous paper, we stated the ratio between the slopes of ω_{AF}^2 above and below $T_c = 115$ K as -3.4 [15]. This is in disagreement with the prediction of -2 from Table I. It suggested that the displacive transition in francisite is not purely second order, involving elements of a

TABLE I. Eigenmodes of the one-dimensional displacive model described by Eqs. (3)–(5).

	Interaction	Polar mode	Antipolar mode
$T < T_c$	FE	$m\omega_F^2 = -4a$	$m\omega_{AF}^2 = -4a + 4c$
	AFE	$m\omega_F^2 = -4a + 4c$	$m\omega_{AF}^2 = -4a$
$T > T_c$	FE	$m\omega_F^2 = 2a$	$m\omega_{AF}^2 = 2a + 4c$
	AFE	$m\omega_F^2 = 2a + 4c$	$m\omega_{AF}^2 = 2a$

tricritical nature. After reexamining our previous neutron and x-ray diffraction measurements [14,15], we determine that the critical temperature is in fact closer to $T_c = 118$ K. Taking this into consideration, we find the ratio of the slopes for ω_{AF}^2 in the proximity of T_c to be -2.4 ± 0.6, indicating good agreement with the second-order model.

The difference between the squared soft-mode frequencies is shown in Fig. 4(c). As stated above, this relationship is proportional to what can be considered the intersublattice stiffness c. Interestingly, while $c(T)$ remains constant in the paraelectric phase, it exhibits critical behavior in the AFE phase, increasing nonlinearly below T_c. The trend is well fit by a power-law relation $\omega_F^2 - \omega_{AF}^2 = \lambda_0 + \lambda_1 \tau^\beta$, with $\tau = \frac{T_c - T}{T_c}$, $\lambda_0 = 10.7 \pm 2.0$ meV^2, $\lambda_1 = 21.2 \pm 1.7$ meV^2, and critical exponent $\beta = 0.66 \pm 0.17$, consistent with the mean-field universality class.

The tendency for c to increase with a mean-field dependence in the AFE phase is suggestive of an underlying connection to the AFE order parameter. This can be understood in terms of a first-degree Taylor expansion of c with respect to the local ionic displacement $c(x) = c_0 + \frac{\partial c}{\partial x}(x - x_0)$, where $(x_{a,b} - x_0) \propto P_{a,b}$ represents the Kittel sublattice polarization [1]. Intuitively, the local interaction potential confining the displaced ions in antipolar symmetry is reinforced by the molecular field of staggered dipoles in the AFE phase.

In the so-called *modern theory of polarization*, FE order is given a topological interpretation, where electric polarization emerges through the existence of topologically protected boundary charges [31–33]. Extending to higher-order multipoles invokes topological states that describe bulk quadrupoles or octupoles [34]. In this context, it is tempting to consider if a bulk quadrupole moment similar to the cartoon depiction in Fig. 1 could more naturally describe the electric field gradient of staggered dipoles in francisite. Interestingly, investigations of this field gradient were carried out early on in the history of AFEs in the general search for dielectric anomalies surrounding those transitions [35–37]. We anticipate it would be beneficial to revisit those experiments and techniques in light of recent progress in AFE materials.

In conclusion, we have shown foundational work detailing the polar soft-mode dynamics in a model displacive AFE material. The dynamics are in precise agreement with expected behavior, highlighting a close-lying FE phase. By relating experimental observations to the eigenmodes of a simple one-dimensional displacive model, we extract a signature of the sublattice polarization. This analysis is possible in francisite as the key polar and antipolar soft modes are uniquely identified along a single-crystallographic dimension. It will be interesting to see if similar analyses using comprehensive lattice dynamical studies can be applied to other AFEs, a key observation being parallel evolution of ω_F and ω_{AF} above T_c.

[1] C. Kittel, Theory of antiferroelectric crystals, Phys. Rev. **82**, 729 (1951).

[2] L. E. Cross, Antiferroelectric-ferroelectric switching in a simple "Kittel" antiferroelectric, J. Phys. Soc. Jpn. **23**, 77 (1967).

[3] K. Okada, Phenomenological theory of antiferroelectric transition. I. second-order transition, J. Phys. Soc. Jpn. **27**, 420 (1969).

[4] A. P. Levanyuk and D. G. Sannikov, Anomalies in dielectric properties in phase transitions, Zh. Eksp. Teor. Fiz. **55**, 256 (1968) [Sov. Phys.–JETP **28**, 134 (1969)].

[5] L. D. Landau and E. M. Lifshitz, *Electrodynamics of Continuous Media, 2nd edition* (Pergamon, Oxford, 1984).

[6] H. T. Stokes and D. M. Hatch, Model for the ordered phases in KCN and NaCN, Phys. Rev. B **30**, 3845 (1984).

[7] H. Takezoe, E. Gorecka, and M. Čepič, Antiferroelectric liquid crystals: Interplay of simplicity and complexity, Rev. Mod. Phys. **82**, 897 (2010).

[8] P. Tolédano and M. Guennou, Theory of antiferroelectric phase transitions, Phys. Rev. B **94**, 014107 (2016).

[9] T. Fukami, S. Akahoshi, K. Hukuda, and T. Yagi, Refinement of the crystal structure of NH$_4$H$_2$PO$_4$ above and below antiferroelectric phase transition temperature, J. Phys. Soc. Jpn. **56**, 2223 (1987).

[10] S. Horiuchi, R. Kumai, and S. Ishibashi, Strong polarization switching with low-energy loss in hydrogen-bonded organic antiferroelectrics, Chem. Sci. **9**, 425 (2018).

[11] A. K. Tagantsev, K. Vaideeswaran, S. B. Vakhrushev, A. V. Filimonov, R. G. Burkovsky, A. Shaganov, D. Andronikova, A. I. Rudskoy, A. Q. R. Baron, H. Uchiyama, D. Chernyshov, A. Bosak, Z. Ujma, K. Roleder, A. Majchrowski, J.-H. Ko, and N. Setter, The origin of antiferroelectricity in PbZrO$_3$, Nat. Commun. **4**, 2229 (2013).

[12] J. Hlinka, T. Ostapchuk, E. Buixaderas, C. Kadlec, P. Kuzel, I. Gregora, J. Kroupa, M. Savinov, A. Klic, J. Drahokoupil, I. Etxebarria, and J. Dec, Multiple Soft-Mode Vibrations of Lead Zirconate, Phys. Rev. Lett. **112**, 197601 (2014).

[13] J. Íñiguez, M. Stengel, S. Prosandeev, and L. Bellaiche, First-principles study of the multimode antiferroelectric transition in PbZrO$_3$, Phys. Rev. B **90**, 220103(R) (2014).

[14] E. Constable, S. Raymond, S. Petit, E. Ressouche, F. Bourdarot, J. Debray, M. Josse, O. Fabelo, H. Berger, S. deBrion, and V. Simonet, Magnetic and dielectric order in the kagome-like francisite Cu$_3$Bi(SeO$_3$)$_2$O$_2$Cl, Phys. Rev. B **96**, 014413 (2017).

[15] C. Milesi-Brault, C. Toulouse, E. Constable, H. Aramberri, V. Simonet, S. de Brion, H. Berger, L. Paolasini, A. Bosak, J. Íñiguez, and M. Guennou, Archetypal soft-mode-driven antipolar transition in francisite Cu$_3$Bi(SeO$_3$)$_2$O$_2$Cl, Phys. Rev. Lett. **124**, 097603 (2020).

[16] D. A. Prishchenko, A. A. Tsirlin, V. Tsurkan, A. Loidl, A. Jesche, and V. G. Mazurenko, Antiferroelectric instability in the kagome francisites Cu$_3$Bi(SeO$_3$)$_2$O$_2$X (X = Cl,Br), Phys. Rev. B **95**, 064102 (2017).

[17] W. Cochran, Crystal stability and the theory of ferroelectricity, Adv. Phys. **9**, 387 (1960).

[18] W. Cochran, Crystal stability and the theory of ferroelectricity part II. Piezoelectric crystals, Adv. Phys. **10**, 401 (1961).

[19] K. H. Miller, P. W. Stephens, C. Martin, E. Constable, R. A. Lewis, H. Berger, G. L. Carr, and D. B. Tanner, Infrared phonon anomaly and magnetic excitations in single-crystal $Cu_3Bi(SeO_3)_2O_2Cl$, Phys. Rev. B **86**, 174104 (2012).

[20] See Supplemental Material at http://link.aps.org/supplemental/10.1103/PhysRevResearch.5.L012036 for experimental details, supporting measurements, and eigen mode derivation of the AFE model.

[21] C. Geuzaine and J. F. Remacle, Gmsh: A 3-d finite element mesh generator with built-in pre- and post-processing facilities, Int. J. Numer. Methods Eng. **79**, 1309 (2009).

[22] F. Hecht, New development in freefem+, J. Numer. Math. **20**, 251 (2012).

[23] P. J. Frey, Medit : An interactive mesh visualization software, INRIA Tech. Rep. 0253 (2001).

[24] E. Barsoukov and J. R. Macdonald, *Impedance Spectroscopy* (Wiley, Hoboken, NJ, 2005).

[25] E. Constable and R. A. Lewis, Optical parameters of ZnTe determined using continuous-wave terahertz radiation, J. Appl. Phys. **112**, 063104 (2012).

[26] A. A. Volkov, G. V. Kozlov, E. B. Kryukova, and J. Petzelt, Low-temperature transformations of the relaxational soft modes in crystals of the rochelle salt family, Zh. Eksp. Teor. Fiz. **90**, 192 (1986) [Sov. Phys.–JETP **63**, 110 (1986)].

[27] T. Ostapchuk, J. Petzelt, V. Zelezny, S. Kamba, V. Bovtun, V. Porokhonskyy, A. Pashkin, P. Kuzel, M. D. Glinchuk, I. P. Bykov, B. Gorshunov, and M. Dressel, Polar phonons and central mode in antiferroelectric $PbZrO_3$ ceramics, J. Phys.: Condens. Matter **13**, 2677 (2001).

[28] E. Buixaderas, S. Kamba, and J. Petzelt, Lattice dynamics and central-mode phenomena in the dielectric response of ferroelectrics and related materials, Ferroelectrics **308**, 131 (2004).

[29] G. Shirane, E. Sawaguchi, and Y. Takagi, Dielectric properties of lead zirconate, Phys. Rev. **84**, 476 (1951).

[30] W. Cochran, Crystal Stability and the Theory of Ferroelectricity, Phys. Rev. Lett. **3**, 412 (1959).

[31] R. D. King-Smith and D. Vanderbilt, Theory of polarization of crystalline solids, Phys. Rev. B **47**, 1651 (1993).

[32] D. Vanderbilt and R. D. King-Smith, Electric polarization as a bulk quantity and its relation to surface charge, Phys. Rev. B **48**, 4442 (1993).

[33] R. Resta, Macroscopic polarization in crystalline dielectrics: The geometric phase approach, Rev. Mod. Phys. **66**, 899 (1994).

[34] W. A. Benalcazar, B. A. Bernevig, and T. L. Hughes, Electric multipole moments, topological multipole moment pumping, and chiral hinge states in crystalline insulators, Phys. Rev. B **96**, 245115 (2017).

[35] H. v. Einsiedel and S. S. Rosenblum, Electric quadrupole interaction in the phase transition region of antiferroelectric $PbHfO_3$, J. Phys. C: Solid State Phys. **6**, L292 (1973).

[36] H. V. Einsiedel and S. S. Rosenblum, Temperature dependence of the electric quadrupole interaction in $PbZrO_3$, Phys. Status Solidi B **65**, K5 (1974).

[37] Y. Yeshurun, Y. Schlesinger, and S. Havlin, Temperature dependence of the electric quadrupole interaction in $PbHfO_3$, J. Phys. Chem. Solids **40**, 231 (1979).